Characterisation of endogenous Claudin-1 expression, motility and susceptibility to hepatitis C virus in CRISPR knock-in cells.

Camille M H Clément, Maika S Deffieu, Cristina M. Dorobantu, Thomas F. Baumert, Nilda Vanesa Ayala-Nunez, Yves Mely, Philippe Ronde, Raphael Gaudin

Characterization of endogenous Claudin1 expression, motility and susceptibility to Hepatitis C Virus in CRISPR knock-in cells

Camille M.H. Clément[1,2,3,4,#], Maika S. Deffieu[1,2,#], Cristina M. Dorobantu[3,4,$], Thomas F. Baumert[3,4,5], Nilda Vanesa Ayala-Nunez[1,2,3,4], Yves Mély[4,6], Philippe Ronde[4,6], Raphael Gaudin[1,2,3,4*].

[1] CNRS, IRIM Institut de Recherche en infectiologie de Montpellier, 34293 Montpellier, France
[2] Université de Montpellier, 34090 Montpellier, France
[3] Inserm U1110 – Institut de Recherche sur les Maladies Virales et Hépatiques (IVH)
[4] Université de Strasbourg, 67000 Strasbourg, France
[5] Pole Hépato-digestif, Hôpitaux Universitaires de Strasbourg, Institut Hospitalo-universitaire, 67000 Strasbourg, France
[6] CNRS UMR 7021, Laboratoire de Bioimagerie et Pathologies, Faculté de pharmacie, 67401 Illkirch, France.
[$] Present addresses:

CD: Viroclinics Biosciences B.V., Rotterdam, The Netherlands

[#] These authors contributed equally

* Corresponding author:

Raphael Gaudin, PhD
Institut de Recherche en Infectiologie de Montpellier (IRIM)
CNRS UMR9004
1919 route de Mende, 34293 Montpellier, France
Phone: +33 4 34 35 94 78
Email: raphael.gaudin@irim.cnrs.fr
Running title: Endogenous CLDN1 tagging using CRISPR/Cas9

Keywords: Gene editing; permeability; FRAP; hepatocellular carcinoma; claudin; CLDN1; HCV

Abstract

Background Information. Claudin1 (CLDN1) is a four-span transmembrane protein localized at cell-cell tight junctions (TJs), playing an important role in epithelial impermeability and tissue homeostasis under physiological conditions. Moreover, CLDN1 expression is upregulated in several cancers, and the level of CLDN1 expression has been proposed as a prognostic marker of patient survival.

This article has been accepted for publication and undergone full peer review but has not been through the copyediting, typesetting, pagination and proofreading process, which may lead to differences between this version and the Version of Record. Please cite this article as doi: 10.1111/boc.201900085.

Results. Here, we generated and characterized a novel reporter cell line expressing endogenous fluorescent levels of CLDN-1, allowing dynamic monitoring of CLDN-1 expression levels. Specifically, a hepatocellular carcinoma Huh7.5.1 monoclonal cell line was bioengineered using CRISPR/Cas9 to endogenously express a fluorescent TagRFP-T protein fused at the N-terminus of the CLDN1 protein. These cells were proved useful to measure CLDN1 expression and distribution in live cells. However, the cells were resistant to hepatitis C virus (HCV) infection, of which CLDN1 is a viral receptor, while retaining permissiveness to VSV-G-decorated pseudoparticles. Nonetheless, the TagRFP-CLDN1$^{+/+}$ cell line showed expected CLDN1 protein localization at TJs and the cell monolayer had similar impermeability and polarization features as its wild-type counterpart. Finally, using fluorescence recovery after photobleaching (FRAP) approaches, we measured that the majority of endogenous and overexpressed TagRFP-CLDN1 diffuses rapidly within the TJ, whereas half of the overexpressed EGFP-CLDN1 proteins were stalled at TJs.

Conclusions. The Huh7.5.1 TagRFP-CLDN1$^{+/+}$ edited cell line showed physiological features comparable to that of non-edited cells, but became resistant to HCV infection. Our data also highlights the important impact of the fluorescent protein chosen for endogenous tagging.

Significance. Although HCV-related studies may not be achieved with these cells, our work provides a novel tool to study the cell biology of tight-junction associated proteins and a potential screening strategy measuring CLDN1 expression levels.

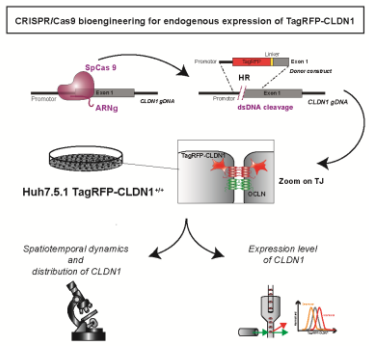

The study by Clément et al generated a new gene edited Huh7.5.1 cell line endogenously expressing the TagRFP-T fluorescent protein fused to CLDN1. This cell line allow live measurement of CLDN1 expression and distribution

Introduction

The Claudin family is composed of 24 members, exhibiting four transmembrane domains: a short amino terminal domain (2-6 residues), two extracellular loops and a C-terminal cytoplasmic tail (for review see (Anderson and Van Itallie, 2009)). Claudins favor cell-to-cell adhesion by homo- or heterotypic interactions with neighboring cells. They are also involved in the maintenance of epithelial/endothelial cell impermeability and confer the ion selectivity of TJs.

Claudin-1 (CLDN1) together with Claudin-2 (CLDN2), were the two first members of the Claudin family discovered (Furuse et al., 1998). CLDN1 knock-out in mice results in expected Mendelian ratios and the newborn animals were indistinguishable from wild-type littermate (Furuse et al., 2002). Although epidermis cytoarchitecture was normal, they died within a day with wrinkled skin, due to dehydration, suggesting that CLDN1 plays a crucial role in the epidermis' homeostasis.

CLDN1 has been particularly investigated in the context of cancer, in which it has been reported to be upregulated in most types of malignancy, including hepatocellular carcinoma, colorectal carcinoma, gastric adenocarcinoma, meningioma, ovarian epithelial carcinoma, pancreatic carcinoma, prostate carcinoma and renal cell carcinoma (Singh et al., 2010). Therefore, CLDN1 expression level has been proposed as a prognostic marker of patient survival in renal cell carcinomas (Fritzsche et al., 2008), although it is highly cancer-type dependent and inverse correlation may also exist (Pyo et al., 2019). CLDN1 plays also a role in the cell entry of the Hepatitis C virus (HCV) (Evans et al., 2007), while other entry factors are also required (Miao et al., 2017). Using constructs to overexpress tagged versions of CLDN1, it was proposed that CLDN1 interacts with CD81 (another HCV entry factor), favoring virus entry (Harris et al., 2010; Harris et al., 2008).

Given its important role in HCV entry, CLDN1 has been shown to be a target for antiviral therapy (Colpitts et al., 2018; Mailly et al., 2015). Furthermore, given the overexpression of CLDN1 in various cancers (Kwon, 2013; Zeisel et al., 2018), CLDN1 has been proposed as target for anti-cancer therapies (Cherradi et al., 2017). The molecular mechanisms involved in the tight regulation of the expression and distribution of Claudins have been well studied (Anderson and Van Itallie, 2009; Tsukita et al., 2019) but strategies to modulate them are still scarce. New tools such as reporter cell lines expressing endogenous levels of CLDN1 under the control of its physiological promoter and within its physiological genomic microenvironment may help to develop innovative therapeutic strategies.

The Clustered Regularly Interspaced Short Palindromic Repeats (CRISPR) has been widely used to surgically insert DNA sequences into the genome of mammalian cells, offering novel

tagging approaches in cell biology and cancer research (Davare and Tognon, 2015). Here we present the first CRISPR/Cas9-engineered cell line, to our knowledge, in which an endogenous TJ-associated protein was fully replaced by a fluorescently-tagged version of the protein.

Results

The overexpression of CLDN1 is associated to increased cell proliferation, invasion and migration and affects epithelial permeability in various cell lines (Zeisel et al., 2018). Therefore, transient transfection of CLDN1 cDNA classically employed to express a tagged version of the protein, may lead to artefacts associated to overexpression. Here, we designed a CRISPR-based approach to generate cells expressing endogenous levels of fluorescently tagged CLDN1. A sequence coding for the fluorescent TagRFP-T protein (Shaner et al., 2008) was inserted at the start codon of the gene coding for CLDN1, followed by a GGSGGSGGS coding sequence to flexibly link the TagRFP-T tag to CLDN1 (Figure 1).

The hepatocellular carcinoma cell line Huh7.5.1 was edited upon transfection with a plasmid coding for the spCas9 protein, a DNA PCR product coding for a guide RNA (gRNA) targeting the ATG region of the CLDN1 gene, and a TagRFP-T "donor" plasmid providing the DNA template for homologous recombination as previously described (Chou et al., 2016; Ran et al., 2013). Flow cytometry cell sorting of single cells provided monoclonal cell lines that were screened by PCR on the extracted genomic DNA. We selected a monoclonal cell line expressing the TagRFP-T tag on all alleles (TagRFP-CLDN1$^{+/+}$), as no endogenous band was detected (Figure 2a). At the protein level, a band at ≈ 22 kDa, corresponding to the expected size was detected for WT cells, while no band was observed at this size for TagRFP-CLDN1$^{+/+}$ cells (Figure 2b). Instead, a higher band at ≈ 49 kDa was observed, corresponding to the expected size of the chimera fusion protein TagRFP-CLDN1. A lower faint band was also observed in both cell types, which may correspond to a CLDN1 isoform. By flow cytometry, all TagRFP-CLDN1$^{+/+}$ cells show high fluorescence as compared to WT cells (Figure 2c). To compare whether the edited cells express the same amount of CLDN1 as their wild-type parental cell line, cells were stained with an anti-CLDN1 antibody and the mean fluorescence intensity (MFI) was measured by flow cytometry. In parallel, GAPDH antibody staining was performed to normalize the general protein expression level per cell. No difference was observed between WT and edited cells (Figure 2d-e), indicating that the addition of TagRFP-T to the CLDN1 protein did not change its expression level.

Using confocal microscopy, we found that TagRFP-CLDN1 strongly colocalized with anti-CLDN1 antibodies (Figure 2f, upper panels), indicating that no cleaved TagRFP-T proteins

exist. The antibody staining was localized at the plasma membrane and intracellularly, which was also found in WT cells (Figure 2f, lower panels), suggesting that a pool of CLDN1 is endocytosed/recycled.

As CLDN1 was proposed to promote liver cancer (Suh et al., 2013), we tested whether the TagRFP-CLDN1$^{+/+}$ edited cells could be used as a reporter cell line to monitor live endogenous CLDN1 protein distribution and localization using confocal microscopy and flow cytometry. We found that treatment with pharmacological inhibitors interfering with tubulin and actin polymerization (nocodazole and latrunculin B respectively), or inducing apoptosis (staurosporin) were all affecting CLDN1 distribution 3 h post-treatment (Figure 3a). Within this time period, latrunculin B and staurosporin treatments induced a significant decrease of CLDN1 protein levels, while nocodazole had no effect (Figure 3b). These observations suggest that the TagRFP-CLDN1$^{+/+}$ edited cell line could be used for drug screening.

CLDN1 is also an important entry factor required for successful infection of the Hepatitis C virus (HCV). Therefore, the TagRFP-CLDN1$^{+/+}$ edited cell line could prove useful to study HCV-CLDN1 interactions. The permissiveness of these cells to replication-competent recombinant HCV grown in cell culture (HCVcc) expressing the luciferase reporter was tested. Surprisingly, these cells became fully resistant to the infection by HCVcc, while VSV-G pseudoparticles were not significantly impacted by the editing (Figure 4).

We wondered whether tagging CLDN1 could affect cell polarity and impermeability. By confocal microscopy, we showed that TagRFP-CLDN1 distributed at TJs together with Occludin (OCLN), another TJ-associated protein (Figure 5a, upper panel). Moreover, the edited cells were similarly polarized as WT cells as observed by the apical localization of the Ezrin staining (Figure 5a, lower panel). To test for impermeability of the epithelial monolayer, cells were grown for four days on a transwell insert harboring a membrane with 0.4 µm pores (Figure 5b). The cell monolayers' relative permeability measured by transepithelial electrical resistance (TEER) using a Voltohmmeter was similar for the WT and edited cells (Figure 5c). As TEER may not account for subtle differences, cells grown as in Figure 5b were subjected to the fluorescent fluid phase marker Lucifer Yellow. The amount of Lucifer yellow in the lower chamber, compared to the one retained in the upper chamber was measured on a fluorometer and a permeability coefficient was calculated (see Methods for details). As previously observed with TEER, the WT and edited cells did not exhibit significant differences in permeability, while incubation with EDTA was lowering epithelial impermeability in both cell lines (Figure 5d).

Finally, we tested whether the tag could interfere with the localization and diffusive properties of CLDN1. To this end, we compared the TagRFP-CLDN1$^{+/+}$ edited cells to cells transiently overexpressing CLDN1 fused in N-terminal to EGFP or TagRFP. First, we found that overexpressing CLDN1 led to a strong increase of the intracellular pool of CLDN1, which may represent artefactual endosomes loaded with CLDN1 excess (Figure 6a). Focusing on plasma membrane-localized CLDN1, we performed live cell imaging and fluorescent recovery after photobleaching (FRAP) experiments to measure the diffusion behavior of CLDN1 according to the tag and protein expression level. A representative FRAP time lapse shows CLDN1 fluorescence signal before (0 s), right after (13 s) and at later time-point post-bleaching (Figure 6b). Analyzes of the $T_{1/2}$ did not show significant differences (Figure 6c). Of note, the analysis was difficult due to the large number of intracellular vesicles in the cytosol and only a few movies were analyzable and used for quantification. Moreover, we cannot exclude that several CLDN1 mobile behaviors co-exist. This is particularly true with EGFP-CLDN1 overexpressing cells where the FRAP curves could be fitted with two or more exponentials, which may have given further behavior insights (although their interpretation may have been complex). Finally, the fluorescence recovery of the mobile fraction was nearly total for the endogenous and overexpressed TagRFP-CLDN1, while only about half of the overexpressed EGFP-CLDN1 was mobile (Figure 6d). This surprising result highlights that CLDN1 diffusion may be impacted depending on the fluorescent protein fused to it.

Discussion

We generated a novel cell line and associated pipeline, which strategy could be repurposed to monitor other reporter proteins. Of note however, the editing efficiency was low (≈ 0.5%), which is common when one tries to insert large DNA fragments using homologous recombination (HR). Improved CRISPR-based knock-in methods have been released based on non-homologous end joining (NHEJ), which could further facilitate and fasten this process (Sawatsubashi et al., 2018; Suzuki et al., 2016). Yet, the constraints associated to the design of the adequate target sequence confer complexity to these novel editing strategies.

Here, using antibody staining coupled to flow cytometry, we found that expression of CLDN1 was not impacted by endogenous tagging. Of note however, a decreased intensity of the TagRFP-CLDN1 band was observed by western blot, compared to wild type CLDN1 (Figure 2b). We attributed this difference to the lower transfer efficiency of proteins with higher molecular weight, precluding proper quantification of the protein expression levels. Indeed, flow cytometry experiments confirmed that CLDN1 expression was not impacted by the

addition of the tag (Figure 2d-e). By microscopy, we observed that CLDN1 was mainly localized at TJs, as expected for a Claudin family member. However, a subset of CLDN1 proteins was also observed outside TJs, a distribution that is not so surprising, as Claudins also exert numerous “non-canonical” functions (Hagen, 2017; Van Itallie and Anderson, 2013).

CLDN1 expression has been proposed for cancer prognosis (Fritzsche et al., 2008) and our work provides a novel approach to quantitatively assess it in live cells. Moreover, anti-CLDN1 antibodies have been proposed for colorectal cancer therapy and antiviral HCV treatment (Cherradi et al., 2017; Mailly et al., 2015), but their mode of action remains only partially understood. Here, the TagRFP-CLDN1 edited cells provide a powerful platform to study small molecule inhibitors and could also be used to evaluate the anti-cancerous and antiviral properties of CLDN1-targeting compounds. Furthermore, pharmacologic and genetic screens could also be setup using these cells to quickly and reliably assess CLDN1 expression and distribution in a dynamic manner.

CLDN1 plays a role in the cell entry of the Hepatitis C virus (HCV) (Evans et al., 2007), while other entry factors are also required (Miao et al., 2017). Using constructs to overexpress N-terminus tagging of CLDN1, it was proposed that CLDN1 interacts with CD81 (another HCV entry factor), favoring virus entry (Harris et al., 2010; Harris et al., 2008). Here, we found that the cells lost permissiveness for unknown reasons. A possibility is that the TagRFP protein is affecting the cytosolic interactions between CLDN1 and other HCV entry factors, such as CD81 for instance. This could preclude the formation of the HCV entry receptor complex at the plasma membrane. Further work would be required to decipher the importance of these findings.

The cytosolic N-terminal region of CLDN1 is predicted to be only 7 amino acid long and thus, this position was previously used to tag the Claudin proteins (Harris et al., 2008; Shen et al., 2008; Van Itallie et al., 2017). The previous reports only used overexpressed proteins, and endogenous CLDN1 remained. Here, by endogenously tagging CLDN1, we show that the N-terminal labeling of the protein does not perturb cell impermeability or cell polarity (Figure 5). We found that endogenous TagRFP-CLDN1 was highly mobile at TJs with fast fluorescence recovery rates compared to previously published data (Shen et al., 2008). Several explanations could explain these differences: the cell line used (human hepatocellular carcinoma versus Madin-Darby Canine Kidney (MDCK) cells), the fused protein (TagRFP-T versus EGFP), and the expression strategy (CRISPR versus transient overexpression). However, EGFP-CLDN1^{overexp} showed diffusion properties that were closer to the previous

study, with half of the FRAP CLDN1 being stalled at TJs (Figure 6d). These results point out toward a strong influence of the fluorescent protein fused to CLDN1 and it remains unclear which diffusion behavior CLDN1 adopts in wild-type conditions. Analyses of more fluorescent proteins and the use of smaller tags would help understanding these discrepancies.

Materials and Methods

Cell line

The hepatocellular carcinoma Huh7.5.1 cell line (Zhong et al., 2005) was cultured in Dulbecco's Modified Eagle's Medium (DMEM) containing 4.5 g/L D-Glucose (Gibco) supplemented with 10% fetal bovine serum (Sigma-Aldrich), 1X MEM non-essential amino acids (Gibco), and 1X gentamicin (10 mg/mL; Gibco).

Antibodies

Rabbit anti-CLDN1 antibody from Elabscience was used in flow cytometry and polyclonal rat anti-CLDN1 antibody previously described (Krieger et al., 2010), was used for microscopy experiments. Mouse anti-GAPDH antibody [GT239] and Rabbit anti-Ezrin antibody were purchased form GenTex. Mouse anti-OCLN antibody and donkey anti-mouse/rabbit Alexa Fluor 488 and 647 were purchased from Thermofisher Scientific. Goat anti-mouse IgG antibody coupled to HRP and anti-rabbit IgG antibody coupled to HRP were purchased from Jackson ImmunoResearch. Mouse anti-beta Actin antibody [AC-15] was purchased from Abcam. Rabbit IgG conjugated to Alexa Fluor 647 (isotype control) was purchased from R&D System.

Plasmids

Plasmids coding EGFP-CLDN1 and TagRFP-CLDN1 were amplified from gblock sequences (IDTDNA). The primers used to amplify the gBlock sequences are the following:

TagRFP-forward	5'-GTCAGCGGCCGCCTCGAGCGATGGTGTCTAAGGGCGAA-3'
EGFP Forward	5'-GTCAGCGGCCGCCTCGAGCGATGGTGAGCAAGGGCGA-3'
CLDN1 Reverse	5'-GTCAGGATCCTCACACGTAGTCTTTCCCG-3'

The PCR fragments are flanked with Not1 and BamH1 restriction enzymes to be cloned into a pHAGE IRES-puromycin plasmid.

Crispr/Cas9 knock-in

F1 upstream CLDN1 ATG	5' – gaattcgagctcggtacccGTGTGTGTGTAAATCATGTTGCTCTC – 3'

R1 upstream CLDN1 ATG	5’ – gactcgctcgggcgccc – 3’
F2 upstream CLDN1 ATG TagRFP	5’ – ggcgcccgagcgagtcATGGTGTCTAAGGGCGAAGAGC – 3’
R2 TagRFP	5’ – ggaaccaccagaaccaccagaacc – 3’
F3 linker downstream CLDN1 ATG	5’ – ggtggttctggtggttcccTGGCCAACGCGGGGCTGC – 3’
R3 downstream CLDN1 ATG	5’ – gtcgactctagaggatccccGCAGCTTCTCCAAAGAGTCTTGC – 3’

The “donor construct” used as template for the homologous recombination step was generated by fusion of two ~800-nucleotide fragments of genomic DNA upstream and downstream of the ATG start codon of CLDN1 and the open reading frame of TagRFP-T (see Figure 1). The primers used to generate these 3 fragments are described below (upper and lower cases indicate different targeting sequences):

The genomic fragments were obtained by two independent PCR amplifications using the genomic DNA (gDNA) of Huh7.5.1 cells extracted using the QuickExtract DNA extraction solution (Lucigen) as template and the F1-R1 and F3-R3 primers. The sequence coding for TagRFP-T followed by the GGS linker was amplified using the F2-R2 primers. The three PCR products were introduced into pUC19 vector by Gibson assembly (NEB) strategy and verified by DNA sequencing (Eurofins genomics).

The guide RNA of sequence 5’–GAGCGAGTCATGGCCAACGC–3’ was designed using the crispr.mit.edu website. A PCR on a plasmid containing the U6 promoter with U6 forward primer 5’–ACGGGCCAGATATACGCGTTAAGGTCGGGCAGGAAGAGGG–3’ and long reverse primer containing the gRNA and tracrRNA sequences was purchased as ultramer from IDTDNA and had the following sequence:

5-
’ACCTCTAGAAAAAAAGCACCGACTCGGTGCCACTTTTTCAAGTTGATAACGGACTAGCC
TTATTTTAACTTGCTATTTCTAGCTCTAAAACGCGTTGGCCATGACTCGCTCCGGTGTTT
CGTCCTTTCCACAAG – 3’. Electrophoresis of the PCR product was run on a 2% low melting agarose (Invitrogen) gel and purified using NucleoSpin Gel and PCR Clean-up (Macherey-Nagel) according to the manufacturer’s instructions.

Huh7.5.1 cells were plated in 6-well plates to reach 70% confluence on the next day for transfection. Cells were co-transfected with 700 ng of each of the following DNA elements: the “donor” plasmid, the purified PCR product coding for the gRNA-tracrRNA, and a plasmid coding for *Streptococcus pyogenes* Cas9 (spCas9) using JetPrime (Polyplus Transfection) according to manufacturer’s instructions. Upon recovery, cells were detached and seeded on

larger dishes according to their growth rate. At ≈ 15-days post-transfection, cells were detached, resuspended in OptiMEM (Gibco) supplemented with 1% fetal bovine serum (Sigma-Aldrich), 10mM HEPES (Gibco) and filtered through a 40 µm sterile cell strainer (BD Biosciences). Cells were sorted by fluorescence-activated cell sorting (FACS) using a FACSAria 2 (BD Biosciences) instrument equipped with a 561 nm laser and a 130 µm nozzle. An initially low number of cells (~ 0.2%) showed a fluorescent signal above background and two subsequent sorts were required to obtain a pool of ~ 70% of fluorescent edited cells (Figure 2c). Generation of the monoclonal TagRFP-CLDN1$^{+/+}$ cell line was obtained by limit dilution in 96-well plates and grown using filtered media from supernatant of Huh7.5.1 cell culture mixed at a 1:1 ratio with fresh complete media to stimulate the growth.

The gDNA of the monoclonal cell lines was extracted by QuickExtract DNA extraction solution (Lucigen). Identification of the double edited a TagRFP-CLDN1$^{+/+}$ clone was performed by PCR amplification using GoTaq Polymerase (Promega) using primers F_{gCLDN1} 5' – CGGAGCTGCTTTAAATCGCGG – 3' and R_{gCLDN1} 5' – CTGGGCGGTCACGATGTTG – 3' mapping a region around the start codon of *CLDN1*. The amplification of non-edited *CLDN1* corresponds to a 409-bp product, whereas the insertion of TagRFP results in a 1165-bp product.

Western blot

Wild-type and TagRFP-CLDN1$^{+/+}$ Huh7.5.1 cells were lysed in RIPA Buffer (Sigma-Aldrich) for 20 min on ice. Lysates were cleared by centrifugation at 10 000 g for 20 min at 4°C before transferring the supernatant to new tubes. The protein content in the lysates was measured using Pierce BCA protein assay kit (Thermofisher Scientific) according to the manufacturer's instructions. Twenty micrograms of each lysate were loaded on denaturing 4%-12% NuPAGE Bis-Tris protein gels (Invitrogen) and ran under non-reducing conditions. Transfer onto nitrocellulose membranes (Invitrogen) was achieved using a iBlot2 gel transfer device (Invitrogen). Membranes were blocked for 1 h at RT using 5% milk, 0.05% Tween20 in PBS (Genaxxon Bioscience) and subsequently incubated overnight at 4°C with primary antibody in 0.5% milk and 0.05% Tween20 in PBS. The membranes were extensively washed in 0.05% Tween20 in PBS and incubated for 2 h with a solution containing a secondary antibody coupled to the horseradish peroxidase (HRP). Membranes were revealed by chemiluminescence using Clarity Western ECL blotting substrates (Bio-Rad) and images were acquired using a ChemiDoc Touch system (Bio-Rad).

Flow cytometry

Cells detached with Trypsin-EDTA (Gibco) or with 10 mM EDTA (Invitrogen) for plasma membrane protein detection, were centrifuged at 450 g for 5 min at RT, washed once with PBS (Gibco) and fixed for 20 min at RT with 4% paraformaldehyde (PFA). Cells in suspension were incubated in blocking/permeabilization buffer (0.1% Triton X-100 and 0.5% BSA in PBS) for 30 min at RT. Cells were incubated with primary antibodies 2 h at RT, followed by washes and incubation with fluorophore-conjugated secondary antibodies diluted in blocking buffer for 45 min at RT.

For detection of the amount of total TagRFP-CLDN1 following drug treatment, cells were detached with 5 mM EDTA (Invitrogen) for 3 min. Cells were centrifuged at 800 g for 5 min and fixed with 4% PFA for 20 min at room temperature. Cells were washed three times with PBS and they were resuspended in PBS containing 0.5% BSA and 0.5 mM EDTA.

The percentage of positive cells and the mean fluorescence intensity (MFI) were determined by flow cytometry using a Novocyte cytometer (ACEA Biosciences) and results were analyzed using FlowJo (LLC) v10.

Immunostaining and imaging of fixed samples

Cells were grown on 12 mm diameter #1.5 glass coverslips (Electron Microscopy Sciences) in 24-well plates for 48 h. Cells were fixed for 20 min at RT in 4% PFA. The coverslips were incubated in blocking/permeabilization buffer (0.5% BSA and 0.1% Triton X100 in PBS) for 30 min at RT and primary antibodies were then added for 2 h at RT. Upon washes, the coverslips were incubated with fluorophore-conjugated secondary antibodies diluted in blocking/permeabilization buffer for 45 min at RT. Dapi was added 5 min prior coverslip washing and mounting using Fluoromount aqueous mounting medium (Sigma-Aldrich).

Image acquisition was performed using a Z1 inverted microscope (Nikon) mounted with a spinning disk head CSU-X1 (Andor), an EMCCD iXon897 camera (Andor) and a X100 Plan Apo lambda 1.45 NA oil objective (Nikon) controlled by the iQ3 software (Oxford instrument Andor). Images were analyzed with Imaris v.9.2 (Bitplane) or the Fiji version of ImageJ.

Drug treatments

For immunofluorescent and flow cytometry studies, cells were treated with 1 µM nocodazole (Sigma-Aldrich), 2 µM staurosporin (Sigma-Aldrich) and 2 µM latrunculin B (Sigma-Aldrich) for 3 h in regular cell culture medium.

Live cell imaging

Cells were grown on 30 mm diameter #1.5 glass coverslip (Lordil) in 6-well plates for 48 h. Prior imaging, cells were incubated with Draq5 (Fisher Scientific) according to the manufacturer's instructions in Fluorobright media (Gibco) supplemented with 2% FBS (Sigma-Aldrich). Image acquisition was performed using an AxioObserver.Z1 inverted microscope (Zeiss) mounted with a spinning disc head (Yokogawa), a back-illuminated EMCCD camera (Evolve, Photometrics) and a X100, 1.45 NA oil objective (Zeiss) controlled by Visiview v.3.3.0 software (Visitron Systems).

FRAP

FRAP experiments were done on an inverted TIRF microscope (Nikon) using a back-illuminated EMCCD camera (Evolve512, Photometrics) and a X100 APO, 1.49 NA oil objective controlled by Metamorph, and an iLas^2 FRAP/TIRF module (BioVision Technologies). During acquisition, cells were maintained at 37°C in a 5% CO_2 humidified atmosphere using an environmental control system (Okolab). Images were recorded 20 s before bleaching at an interval of 1s. The laser perturbation was set at 40 ms and a 1.6 µm of diameter region was defined to be bleached. At post-bleaching, images were acquired every 1 s to monitor the fluorescence recovery until 200 s.

Impermeability assays

Cells were cultured for 4 days on a 24-well transwell polyester membrane cell culture insert with 0.4 µm pores (Corning). TEER was measured using EVOM2 Epithelial Voltohmmeter (World precision instruments) and STX3 electrodes dipped into the upper and lower chambers of the transwell. The TEER values reported in Ω/cm² correspond to the transwell area multiplied by the measured resistance (Ω).

For the fluorescence-based permeability assay, cells grown in transwells were incubated with 50 µM Lucifer yellow reagent (Merck) added in the top chamber for 2 h at 37°C and media were collected from the top and bottom chambers. Fluorescence quantification was performed using a Mithras LB 940 multimode microplate reader (Berthold Technologies) with 488 nm excitation and a 520 nm emission filter. In parallel, a calibration curve was prepared using Lucifer yellow concentrations of 50, 25, 12.5 or 6.25 µM. The permeability coefficient (Pc) was calculated as follows:

$$Pc = \frac{Volume\,basal\,chamber}{Area\,transwell \times Initial\,concentration\,insert} \times \frac{Final\,concentration\,well}{Time}$$

Virus production and titration

The HCVcc full length RNA was generated using the Megascript T7 transcription kit (ThermoFisher Scientific) according to the manufacturer's instructions. Huh7.5.1 cells were incubated with 5 µg of RNA diluted into Ingenio electroporation solution (Mirus) and electroporated using the T-001 program of the Amaxa nucleofector (Lonza). Viral supernatants were collected every 48 h after up to 6 passages after electroporation. The virus-containing supernatant was centrifuged at 1500 rpm 5 min to eliminate cell debris and the virus production was concentrated 6-10 times on Vivaspin20 centrifugal concentrators with 100 kDa cut-off (Sartorius) and stored at -80°C.

To produce VSV pseudoparticles, HEK 293T cells were seeded in a 10 cm diameters petridish and transfected the day after using Calcium phosphate kit (Ozyme) with a vector coding for the retroviral Gag and Pol proteins, a vector coding for a Luciferase reporter protein inserted in between two LTR HIV sequences and a vector coding for the envelope glycoprotein of VSV (VSV-G).

The viruses were titrated on Huh7.5.1 cells infected for 72 hours at 37°C and 5% CO_2. Cells were lysed using 50 µL Glo lysis buffer (Promega). Luciferase expression was measured using the ONE-Glo luciferase assay system (Promega) in a 96-well flat bottom white plate (Corning) using the Infinite F200 Pro plate reader (Tecan).

Statistical analysis

Statistical analyses of the data were performed using two-tailed unequal variance Student t-tests (ns $p>0.05$, * $p<0.05$, ** $p<0.01$, *** $p<0.001$) and the mean and standard deviation of the mean were plotted using Prism. Number of independent experiments (n) is indicated in each figure legend.

Author contribution

C.M.H.C and C.M.D generated the CRISPR/Cas9 edited cell lines. C.M.H.C characterized the edited cell lines. N.V.A.N optimized the permeability assays. P.R, M.S.D and C.M.H.C performed and analyzed the FRAP. M.S.D generated TagRFP-CLDN1 and EGFP-CLDN1 plasmids for FRAP experiments. M.S.D performed the drug experiments on the edited TagRFP-CLDN1. T.F.B and Y.M provided expertise and reagents. R.G designed and supervised the experiments and wrote the manuscript. All authors edited and commented on the manuscript.

Acknowledgements

We would like to acknowledge the MRI imaging facility of advice and training. This work was supported by an ATIP-AVENIR starting grant to R.G. The salary of C.M.H.C was supported by INSERM and the Region Grand-Est. C.M.D was supported by an EMBO Long Term Fellowship (EMBO ALTF 1428-2016). The research leading to these results has received funding from the People Program (Marie Curie Actions) of the European Union's Seventh Framework Program (FP7/2007-2013) under REA grant agreement n. PCOFUND-GA-2013-609102, through the PRESTIGE program coordinated by Campus France, and from the French Agency for Research on AIDS and Viral Hepatitis (ANRS), both attributed to NVAN. Y.M. and T.F.B are grateful to the Institut Universitaire de France (IUF) for support and providing additional time to be dedicated to research. TFB is the recipient of an ERC AdG (HEPCIR grant agreement N° 667273) and acknowledges funding through LabEx HepSYS (ANR-10-LABX-0028_HEPSYS) and Fondation ARC pour la recherche sur le cancer (grant n° IHU201901299).

References

Anderson, J.M., and Van Itallie, C.M. (2009). Physiology and function of the tight junction. Cold Spring Harbor perspectives in biology 1, a002584.

Cherradi, S., Ayrolles-Torro, A., Vezzo-Vie, N., Gueguinou, N., Denis, V., Combes, E., Boissiere, F., Busson, M., Canterel-Thouennon, L., Mollevi, C., *et al.* (2017). Antibody targeting of claudin-1 as a potential colorectal cancer therapy. J Exp Clin Cancer Res 36, 89.

Chou, Y.Y., Cuevas, C., Carocci, M., Stubbs, S.H., Ma, M., Cureton, D.K., Chao, L., Evesson, F., He, K., Yang, P.L., *et al.* (2016). Identification and characterization of a novel broad spectrum virus entry inhibitor. Journal of virology.

Colpitts, C.C., Tawar, R.G., Mailly, L., Thumann, C., Heydmann, L., Durand, S.C., Xiao, F., Robinet, E., Pessaux, P., Zeisel, M.B., *et al.* (2018). Humanisation of a claudin-1-specific monoclonal antibody for clinical prevention and cure of HCV infection without escape. Gut 67, 736-745.

Davare, M.A., and Tognon, C.E. (2015). Detecting and targetting oncogenic fusion proteins in the genomic era. Biol Cell 107, 111-129.

Evans, M.J., von Hahn, T., Tscherne, D.M., Syder, A.J., Panis, M., Wolk, B., Hatziioannou, T., McKeating, J.A., Bieniasz, P.D., and Rice, C.M. (2007). Claudin-1 is a hepatitis C virus co-receptor required for a late step in entry. Nature 446, 801-805.

Fritzsche, F.R., Oelrich, B., Johannsen, M., Kristiansen, I., Moch, H., Jung, K., and Kristiansen, G. (2008). Claudin-1 protein expression is a prognostic marker of patient survival in renal cell carcinomas. Clin Cancer Res 14, 7035-7042.

Furuse, M., Fujita, K., Hiiragi, T., Fujimoto, K., and Tsukita, S. (1998). Claudin-1 and -2: novel integral membrane proteins localizing at tight junctions with no sequence similarity to occludin. The Journal of cell biology 141, 1539-1550.

Furuse, M., Hata, M., Furuse, K., Yoshida, Y., Haratake, A., Sugitani, Y., Noda, T., Kubo, A., and Tsukita, S. (2002). Claudin-based tight junctions are crucial for the mammalian epidermal barrier: a lesson from claudin-1-deficient mice. The Journal of cell biology 156, 1099-1111.

Hagen, S.J. (2017). Non-canonical functions of claudin proteins: Beyond the regulation of cell-cell adhesions. Tissue Barriers 5, e1327839.

Harris, H.J., Davis, C., Mullins, J.G., Hu, K., Goodall, M., Farquhar, M.J., Mee, C.J., McCaffrey, K., Young, S., Drummer, H.*, et al.* (2010). Claudin association with CD81 defines hepatitis C virus entry. The Journal of biological chemistry 285, 21092-21102.

Harris, H.J., Farquhar, M.J., Mee, C.J., Davis, C., Reynolds, G.M., Jennings, A., Hu, K., Yuan, F., Deng, H., Hubscher, S.G.*, et al.* (2008). CD81 and claudin 1 coreceptor association: role in hepatitis C virus entry. Journal of virology 82, 5007-5020.

Krieger, S.E., Zeisel, M.B., Davis, C., Thumann, C., Harris, H.J., Schnober, E.K., Mee, C., Soulier, E., Royer, C., Lambotin, M.*, et al.* (2010). Inhibition of hepatitis C virus infection by anti-claudin-1 antibodies is mediated by neutralization of E2-CD81-claudin-1 associations. Hepatology 51, 1144-1157.

Kwon, M.J. (2013). Emerging roles of claudins in human cancer. International journal of molecular sciences 14, 18148-18180.

Mailly, L., Xiao, F., Lupberger, J., Wilson, G.K., Aubert, P., Duong, F.H., Calabrese, D., Leboeuf, C., Fofana, I., Thumann, C.*, et al.* (2015). Clearance of persistent hepatitis C virus infection in humanized mice using a claudin-1-targeting monoclonal antibody. Nature biotechnology 33, 549-554.

Miao, Z., Xie, Z., Miao, J., Ran, J., Feng, Y., and Xia, X. (2017). Regulated Entry of Hepatitis C Virus into Hepatocytes. Viruses 9.

Pyo, J.S., Kim, N.Y., and Cho, W.J. (2019). Prognostic Role of Claudin-1 Immunohistochemistry in Malignant Solid Tumors: A Meta-Analysis. J Pathol Transl Med 53, 173-179.

Ran, F.A., Hsu, P.D., Wright, J., Agarwala, V., Scott, D.A., and Zhang, F. (2013). Genome engineering using the CRISPR-Cas9 system. Nature protocols 8, 2281-2308.

Sawatsubashi, S., Joko, Y., Fukumoto, S., Matsumoto, T., and Sugano, S.S. (2018). Development of versatile non-homologous end joining-based knock-in module for genome editing. Scientific reports 8, 593.

Shaner, N.C., Lin, M.Z., McKeown, M.R., Steinbach, P.A., Hazelwood, K.L., Davidson, M.W., and Tsien, R.Y. (2008). Improving the photostability of bright monomeric orange and red fluorescent proteins. Nature methods 5, 545-551.

Shen, L., Weber, C.R., and Turner, J.R. (2008). The tight junction protein complex undergoes rapid and continuous molecular remodeling at steady state. The Journal of cell biology 181, 683-695.

Singh, A.B., Sharma, A., and Dhawan, P. (2010). Claudin family of proteins and cancer: an overview. J Oncol 2010, 541957.

Suh, Y., Yoon, C.H., Kim, R.K., Lim, E.J., Oh, Y.S., Hwang, S.G., An, S., Yoon, G., Gye, M.C., Yi, J.M.*, et al.* (2013). Claudin-1 induces epithelial-mesenchymal transition through activation of the c-Abl-ERK signaling pathway in human liver cells. Oncogene 32, 4873-4882.

Suzuki, K., Tsunekawa, Y., Hernandez-Benitez, R., Wu, J., Zhu, J., Kim, E.J., Hatanaka, F., Yamamoto, M., Araoka, T., Li, Z.*, et al.* (2016). In vivo genome editing via CRISPR/Cas9 mediated homology-independent targeted integration. Nature 540, 144-149.

Tsukita, S., Tanaka, H., and Tamura, A. (2019). The Claudins: From Tight Junctions to Biological Systems. Trends Biochem Sci 44, 141-152.

Van Itallie, C.M., and Anderson, J.M. (2013). Claudin interactions in and out of the tight junction. Tissue Barriers 1, e25247.

Van Itallie, C.M., Tietgens, A.J., and Anderson, J.M. (2017). Visualizing the dynamic coupling of claudin strands to the actin cytoskeleton through ZO-1. Molecular biology of the cell 28, 524-534.

Zeisel, M.B., Dhawan, P., and Baumert, T.F. (2018). Tight junction proteins in gastrointestinal and liver disease. Gut.

Zhong, J., Gastaminza, P., Cheng, G., Kapadia, S., Kato, T., Burton, D.R., Wieland, S.F., Uprichard, S.L., Wakita, T., and Chisari, F.V. (2005). Robust hepatitis C virus infection in vitro. Proceedings of the National Academy of Sciences of the United States of America 102, 9294-9299.

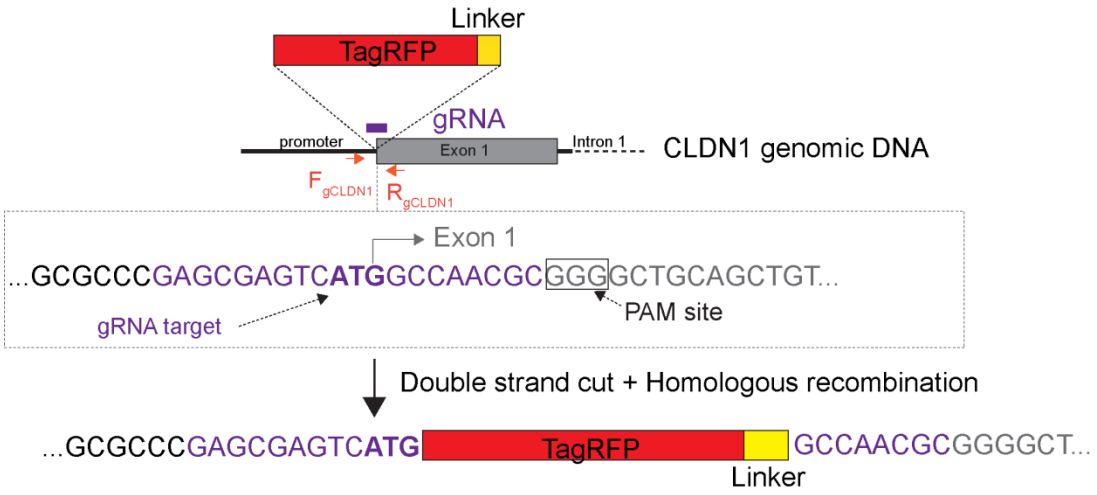

Figure 1. Clément *et al.*

Figure 1. Generation of Huh7.5.1 TagRFP-CLDN1$^{+/+}$ edited cells by CRISPR-Cas9 engineering. Scheme representing the strategy for the insertion of the TagRFP-linker sequence (red and yellow boxes) at the start codon of the *cldn1* gene using site-specific Crispr/Cas9 endonuclease.

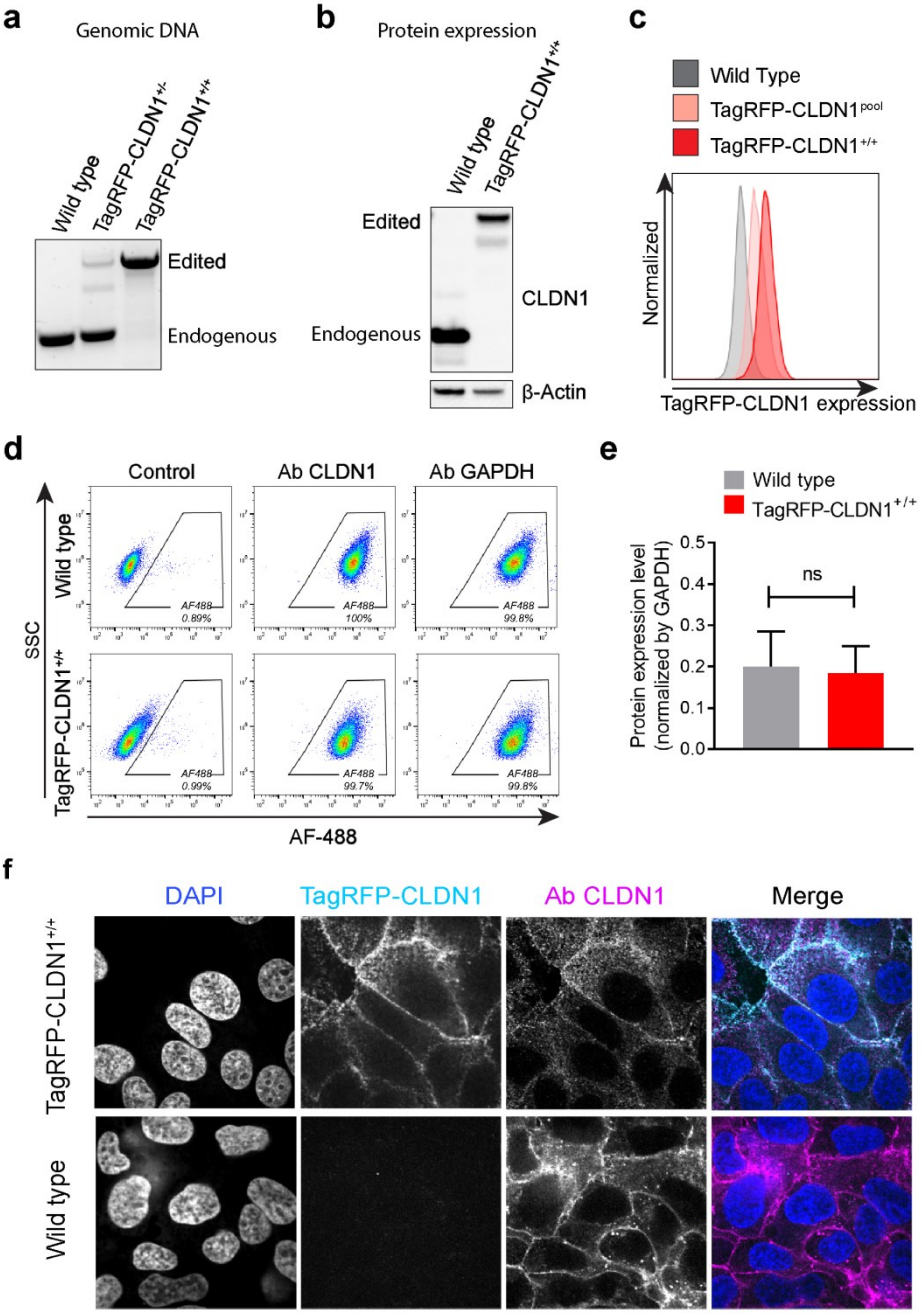

Figure 2. Clément *et al.*

Figure 2. Characterization of the monoclonal TagRFP-CLDN1$^{+/+}$ edited cell line. (a) Genomic PCR analysis using the F_{gCDLN1} and R_{gCLDN1} primers (see red arrows shown in Figure 1). The non-edited *cldn1* gene (endogenous) is seen as a lower band, while the upper band corresponds to the TagRFP sequence inserted into the ATG region of *cldn1* (edited). (b) Western blot analysis of WT and edited cell lysate revealed with an anti-CLDN1 primary antibody and HRP-coupled secondary antibody. The non-edited CLDN1 protein (endogenous) is observed at ≈ 22 kDa in wild type cells. A band at predicted size of ≈ 49 kDa (edited) appears in the TagRFP-CLDN1 edited cells, while endogenous CLDN1 protein band is absent. A β-Actin antibody labeling was used as loading control. (c) The fluorescence of the TagRFP-CLDN1$^{+/+}$ edited cells (red) was detected by flow cytometry

using a 561 nm laser and compared to wild-type (grey) and a pool of edited cells (pink), containing a mix of edited and non-edited cells. (d-e) The absolute amount of CLDN1 protein expression level was measured using an anti-CLDN1 antibody revealed with a A488-coupled secondary antibody and analyzed by flow cytometry. (d) Representative dot plots showing the side-scatter channel as a function of the mean fluorescence intensity measured in the 488 nm laser excitation channel for wild-type (upper panels) or edited cells (lower channel). (e) The mean fluorescence intensity corresponding to the relative CLDN1 protein expressing level was normalized to the mean fluorescence intensity of the GAPDH protein and the mean +/- SD from 3 individual experiments show no difference between wild-type (grey) and edited cells (red). Two-tailed student t-test p value > 0.05 (non-significant; ns). (f) Huh7.5.1 TagRFP-CLDN1$^{+/+}$ (cyan) cells (upper panels) and Huh7.5.1 wild-type cells (lower panels) were fixed, permeabilized and stained using Dapi (blue) and antibody against CLDN1 (magenta). Images were obtained using 3D spinning disk confocal microscopy. The micrographs represent the XY view of a single Z plane.

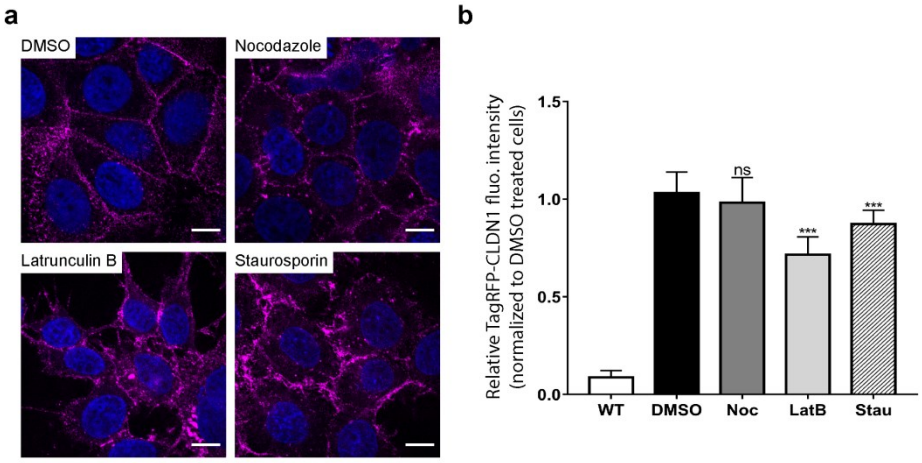

Figure 3. Clément *et al.*

Figure 3. Influence of drug treatment on TagRFP-CLDN1$^{+/+}$ localization and expression. (a) Huh7.5.1 TagRFP-CLDN1$^{+/+}$ cells were seeded on coverslips and treated with DMSO (control), nocodazole (1 µM), latrunculin B (2 µM) or staurosporin (2 µM). At 3 h post treatment, cells were fixed and images were acquired by spinning disk confocal microscopy. The micrographs show representative fluorescence signal of the TagRFP-CLDN1 (magenta) and the nucleus (Blue, Dapi staining). Scale bar = 10 µm. (b) Flow cytometry measurements of the fluorescent level of TagRFP-CLDN1 after the 3-h drug treatment. Wild type cells were used as a control for background fluorescence. The graph represents the ratio of mean fluorescent intensities (MFI) from treated TagRFP-CLDN$^{+/+}$ cells versus mean fluorescent intensities (MFI) from non-treated TagRFP-CLDN$^{+/+}$ cells. n=3 independent experiments from triplicate values for each condition. One-way ANOVA p value was <0.0005 (***).

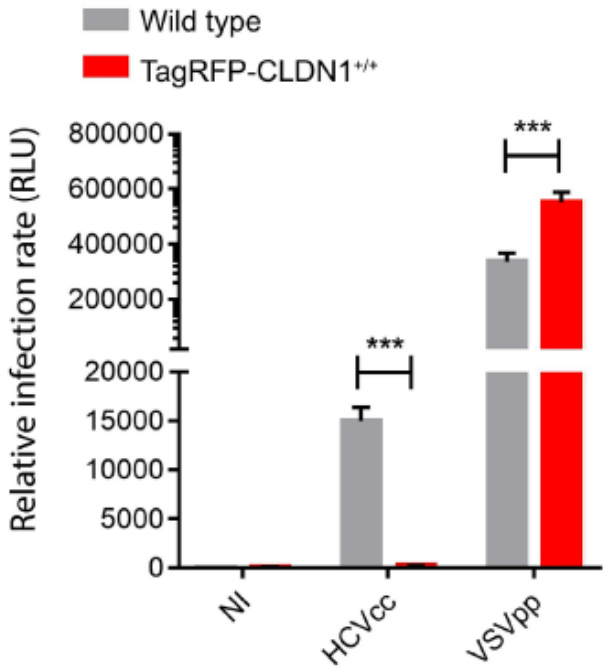

Figure 4. Permissiveness of TagRFP-CLDN1$^{+/+}$ edited cells to HCV. Huh7.5.1 wild type and TagRFP-CLDN1$^{+/+}$ cells were inoculated with the luciferase reporter virus Jc1-Luc strain (HCVcc) or VSV-G-decorated pseudoparticles (VSVpp). Luminescence was measured at 72h post-infection. RLU: Relative luminescence units. The bar graph corresponds to the mean +/- SD from three individual experiments performed in triplicates. Two-tailed p value was < 0.001 (***).

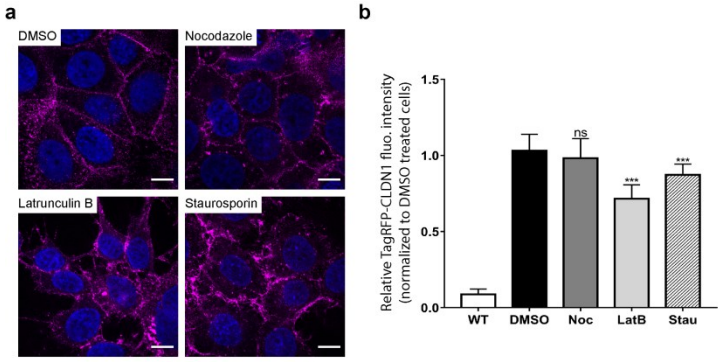

Figure 3. Clément *et al.*

Figure 5. Distribution and impermeability of TagRFP-CLDN1$^{+/+}$ in edited cells. (a) Huh7.5.1 TagRFP-CLDN1$^{+/+}$ (cyan) cells and Huh7.5.1 wild-type cells were fixed, permeabilized and stained using Dapi (blue) and antibodies against OCLN (magenta) and Ezrin (orange). Images were obtained using 3D spinning disk confocal microscopy. The micrographs represent the top view of a Z stack and the lower panels correspond to an orthogonal YZ slice extracted at the pink dotted line. XY and YZ scale bar = 5 µM. (b-d) WT or edited Huh7.5.1 cells were seeded on transwell inserts with 0.4 µm pores for 4 days. (b) Scheme of the transwell system. (c) TEER measurement was performed using a Voltohmmeter. The bar graph corresponds to the mean +/- SD from three experiments performed in duplicate. Two-tailed p value was non-significant (ns) or < 0.001 (***). Edited cells and wild type present a similar TEER value. (d) The medium of the upper chamber in which the cells were grown was replaced by a medium containing 50 µM Lucifer yellow and the permeability coefficient was assessed by measuring the Lucifer Yellow fluorescence intensity in the lower chamber 2 h post-incubation (see Methods for details). EDTA was used as a positive control. The bar graph corresponds to the mean +/- SD from three experiments performed in duplicate. Two-tailed p value was non-significant (ns) or < 0.01 (**) or < 0.001 (***). Both wild-type and edited cells present a low permeability coefficient.

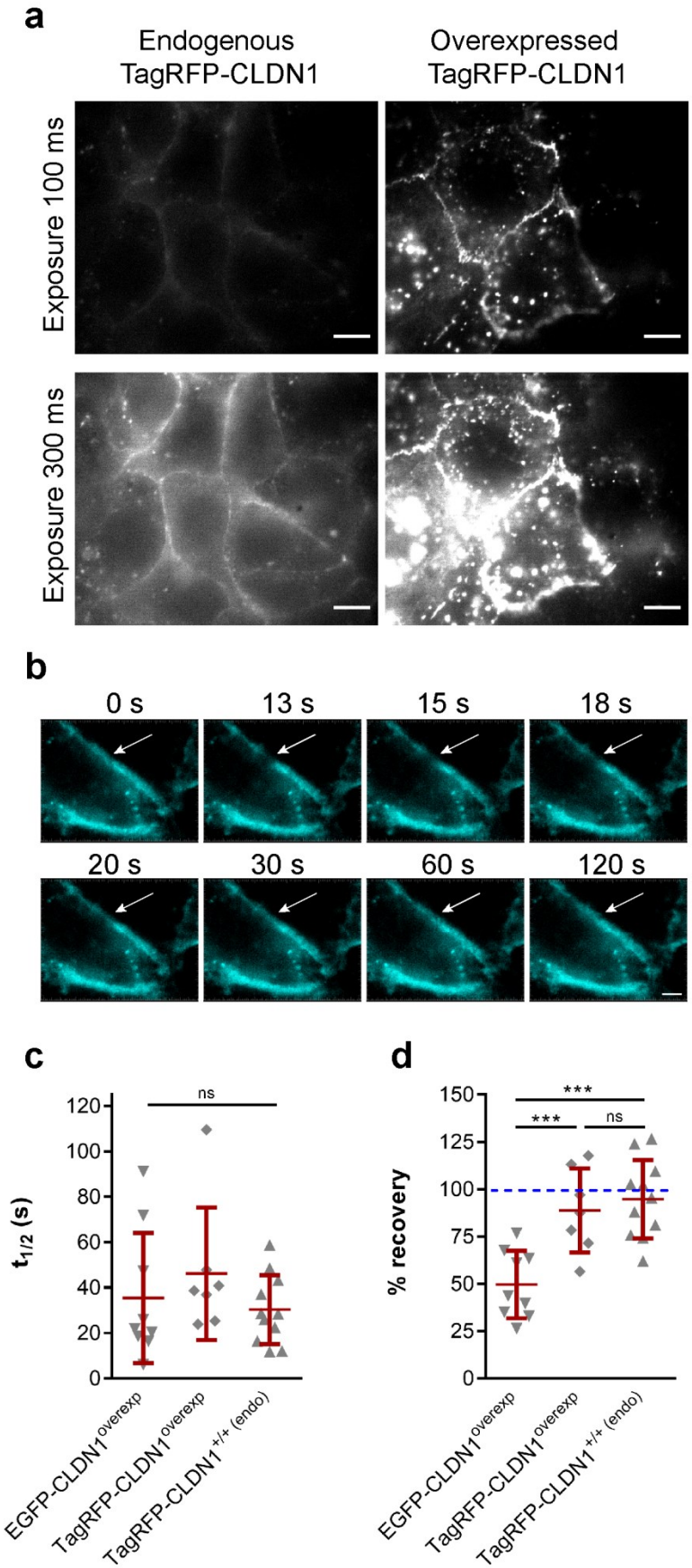

Figure 6. Clément *et al.*

Figure 6. Relative diffusion of CLDN1. (a) Huh7.5.1 TagRFP-CLDN1$^{+/+}$ cells and Huh7.5.1 wild type cells transfected with TagRFP-CLDN1, were seeded on coverslips and imaged by widefield microscopy. The micrographs show representative images of the TagRFP-CLDN1 fluorescence from the indicated cell lines acquired at indicated exposure time, using the same contrasts. Scale bar = 10 µM. (b) Snapshots from a representative time-lapse imaging of TagRFP-CLDN1 (cyan) performed before FRAP (0 s), right after FRAP (13 s) and at indicated times post acquisition. Scale bar = 5 µM. (c-d) The $t_{1/2}$ (c) and percentage of fluorescence recovery (d) +/- SD measured upon TagRFP-CLDN1 photobleaching were calculated. Each dot corresponds to a single movie. Two-tailed p value was non-significant (ns) or < 0.001 (***).